

Detection and Quantification of Creep Strain Using Process Compensated Resonance Testing (PCRT) Sorting Modules Trained with Modeled Resonance Spectra

Julianne Heffernan^{2, b)}, Eric Biedermann^{2, a)}, Alexander Mayes^{2, c)}, Richard Livings^{2, d)}, Leanne Jauriqui^{2, e)}, Brent Goodlet^{3, f)}, John C. Aldrin^{4, g)}, Siamack Mazdiyasni^{1, h)}

¹Air Force Research Laboratory (AFRL/RXCA), Wright-Patterson AFB, OH, USA

²Vibrant Corporation, Albuquerque, NM, USA

³University of California, Santa Barbara, Santa Barbara, CA, USA

⁴Computational Tools, Gurnee, IL, USA

^{a)} Corresponding author: ebiedermann@vibrantndt.com

^{b)} jheffernan@vibrantndt.com

^{c)} amayes@vibrantndt.com

^{d)} rlivings@vibrantndt.com

^{e)} ljauriqui@vibrantndt.com

^{f)} bgoodlet@engineering.ucsb.edu

^{g)} aldrin@computationaltools.com

^{h)} siamack.mazdiyasni@us.af.mil

Abstract. Process Compensated Resonant Testing (PCRT) is a full-body nondestructive testing (NDT) method that measures the resonance frequencies of a part and correlates them to the part's material and/or damage state. PCRT testing is used in the automotive, aerospace, and power generation industries via automated PASS/FAIL inspections to distinguish parts with nominal process variation from those with the defect(s) of interest. Traditional PCRT tests are created through the statistical analysis of populations of “good” and “bad” parts. However, gathering a statistically significant number of parts can be costly and time-consuming, and the availability of defective parts may be limited. This work uses virtual databases of good and bad parts to create two targeted PCRT inspections for single crystal (SX) nickel-based superalloy turbine blades. Using finite element (FE) models, populations were modeled to include variations in geometric dimensions, material properties, crystallographic orientation, and creep damage. Model results were verified by comparing the frequency variation in the modeled populations with the measured frequency variations of several physical blade populations. Additionally, creep modeling results were verified through the experimental evaluation of coupon geometries. A virtual database of resonance spectra was created from the model data. The virtual database was used to create PCRT inspections to detect crystallographic defects and creep strain. Quantification of creep strain values using the PCRT inspection results was also demonstrated.

INTRODUCTION

Resonant Ultrasound Spectroscopy (RUS) correlates the resonance frequencies of a material directly to material elastic properties [1-2]. Process Compensated Resonance Testing (PCRT) is the combination of RUS with advanced pattern recognition algorithms and statistical scoring that measures the resonance frequencies of a part and correlates them to the part's material and/or damage state. PCRT is a well-established nondestructive testing (NDT) method used in the aerospace, power generation, and automotive industries for targeted defect detection, process variation monitoring, and outlier screening [3,4,5]. For instance, Delta Airlines' maintenance division, Delta TechOps, received FAA approval to implement PCRT testing to identify overtemperature conditions in turbine blades [4].

PCRT inspections are created from the statistical analysis of a database of recorded resonance spectra. Within the database, spectra are classified as good or bad based on various nondestructive or destructive evaluations. The classified database, known as the training set, influences the statistical analysis and creation of the targeted inspection. However, cost and availability constraints can make it difficult to obtain well-characterized, statistically significant training populations of acceptable and unacceptable components. PCRT modeling can overcome these data-driven limitations by creating virtual databases of resonance spectra for training PCRT inspections. Prior work has demonstrated that virtual database training sets, created through finite element method (FEM) modeling, can be used to train PCRT inspections to detect and quantify creep strain in simple coupon geometries [6,7].

This work designed and evaluated PCRT inspections for creep and crystal orientation defects from a virtual training database for a complex, representative aerospace turbine blade geometry made from single crystal (SX) nickel-based superalloy, Mar-M-247. Blade populations were modeled using a Monte Carlo (MC) sampling approach to include coupled effects from variations in geometric dimensions, material properties, crystallographic orientation, and creep damage. Model results were verified by comparing the frequency variation in the modeled populations with the measured frequency variations of several physical blade populations. Additionally, the creep modeling technique was verified through the comparison of an experimentally crept sample and modeled creep sample. Quantification of creep strain using PCRT statistical scoring was also evaluated.

PCRT ANALYSIS METHODS

To build a PCRT targeted defect detection inspection (also known as a PASS/FAIL Sorting Module), the resonance spectra from the training sets are analyzed using Vibrational Pattern Recognition (VIPR) algorithms. VIPR uses the Mahalanobis-Taguchi System [8] to score the diagnostic frequency pattern data and optimize which frequencies to use within the Sorting Module. The Mahalanobis Distance [9] calculates the similarity of a given part to the central tendency of the known acceptable (good) population or the similarity to the central tendency of the known unacceptable (bad) population (Bias). The Taguchi component optimizes the number of frequencies used for the calculation, focusing on the most diagnostic frequency patterns rather than using the full broadband spectra.

Figure 1 shows an example of a VIPR plot for a PCRT Sorting Module. The MTS limit (x-axis) is the PASS/FAIL threshold for similarity to the good components (green dots). The Bias limit (y-axis) is the PASS/FAIL threshold for similarity to the bad components. Parts that fall below the MTS and Bias limits pass the PCRT inspection, and parts that exceed either limit (or both) fail. The PCRT system calculates MTS and Bias scores automatically, and returns a PASS/FAIL result that requires no operator interpretation.

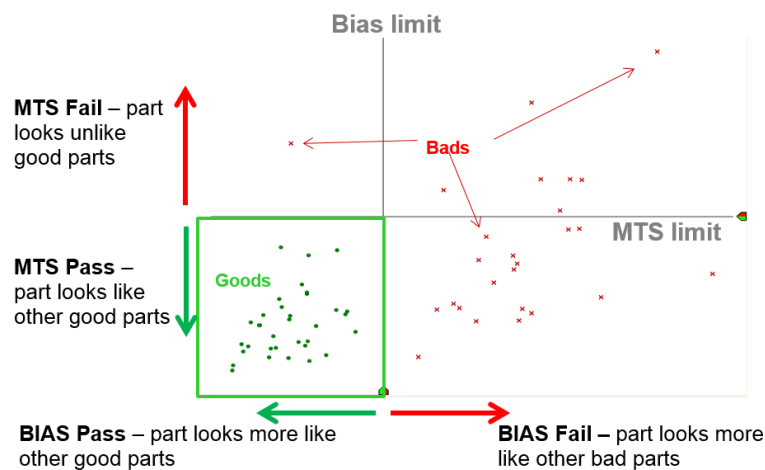


FIGURE 1. VIPR Sorting Module result plot

A robust training set will produce a Sorting Module that is not confounded by nominal production variations while maintaining sensitivity to defects of interest. To create a robust training set, a statistically significant number of good and bad parts are needed. Ideally, the sets will include both the expected variations for the defects (size,

deformation amount, etc.) as well as variations inherent in production (i.e. machine tolerances, material lot variations, etc.).

MODELING

Using FE simulations, a series of forward models of a turbine blade were used to create a robust virtual training set of good and bad parts. The model dimensions were varied for each simulation by creating a parameterized model in SolidWorks [10] and importing each geometry into ANSYS Design Modeler [11]. The material was modeled as a nickel-based superalloy (Mar-M-247), in an anisotropic single crystal (SX) state [6,12]. A Block Lanczos Eigen solver [11] was used to obtain the resonant frequencies for each FE model.

SX crystal orientation was modeled by rotating the local element coordinate system, defined using three angles ω , θ , and P (Fig. 2). Crystallographic alignment for each angle was varied to capture normal and unacceptable orientation variation. For instance, in the good population, the angle (θ) between the (001) crystallographic axis and the long axis of the airfoil was varied 0-15° using a Weibull distribution representing tight casting control [13,14]. In the bad population, θ varied 15-18° to simulate out of nominal casting defects.

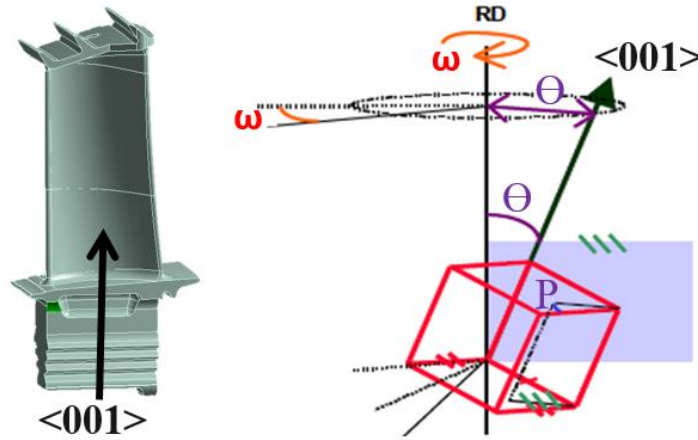


FIGURE 2. Blade model with crystal orientation defined

Creep damage, the time-dependent inelastic deformation of blades, is a common failure mechanism found in turbine blades [15] and was chosen as a primary damage mechanism for this work. The rate of creep deformation is dependent on stress (load), temperature, and time [16]. Instead of a creep modeling approach, which is computationally expensive, a simplified plasticity model was used to model inelastic deformation in a blade. This was an acceptable approximation since both processes result in similar deformations and the residual plastic stress can be removed from the model before the modal analysis step. Previous modeling work has shown that the resulting shape change and frequency response effects from the simplified plasticity model gave similar deformation and frequency results as those from experimental creep tests [6,7,17]. First, the root volume of the blade was fixed and a body acceleration was applied to the full blade to simulate the centripetal acceleration the blade could experience in service. Transverse (perpendicular) loads from aerodynamic pressure on the airfoil were ignored. Second, the acceleration was adjusted to produce varying levels of nonlinear plastic strain as measured along the trailing edge of the blade. Finally, residual stresses were removed from the deformed geometry.

The nonlinear plastic strain was determined through the Hill yield criterion [18] to define the transition from elastic to plastic behavior and a power law hardening rule to define how the yield criterion changes during plastic deformation. The effective yield stress, f , was defined as:

$$f(\sigma, \sigma_y) = F(\sigma_{22} - \sigma_{33})^2 + G(\sigma_{33} - \sigma_{11})^2 + H(\sigma_{11} - \sigma_{22})^2 + 2L\sigma_{23}^2 + 2M\sigma_{31}^2 + 2N\sigma_{12}^2 = 0 \quad (1)$$

where the coefficients are defined as functions of the yield stress ratios (R_{ij}) measured in six different directions [18]:

$$F = \frac{1}{2} \left(\frac{1}{R_{11}^2} + \frac{1}{R_{33}^2} - \frac{1}{R_{11}^2} \right) \quad L = \frac{3}{2} \left(\frac{1}{R_{23}^2} \right) \quad (2,3)$$

$$G = \frac{1}{2} \left(\frac{1}{R_{33}^2} + \frac{1}{R_{11}^2} - \frac{1}{R_{22}^2} \right) \quad M = \frac{3}{2} \left(\frac{1}{R_{13}^2} \right) \quad (4,5)$$

$$H = \frac{1}{2} \left(\frac{1}{R_{11}^2} + \frac{1}{R_{22}^2} - \frac{1}{R_{33}^2} \right) \quad N = \frac{3}{2} \left(\frac{1}{R_{12}^2} \right) \quad (6,7)$$

and R_{ij} are defined by the directional yield stress (σ_{ij}):

$$R_{11} = \left(\frac{\sigma_{11}^y}{\sigma_y} \right) \quad R_{12} = \sqrt{3} \left(\frac{\sigma_{12}^y}{\sigma_y} \right) \quad (8,9)$$

$$R_{22} = \left(\frac{\sigma_{22}^y}{\sigma_y} \right) \quad R_{23} = \sqrt{3} \left(\frac{\sigma_{23}^y}{\sigma_y} \right) \quad (10,11)$$

$$R_{33} = \left(\frac{\sigma_{33}^y}{\sigma_y} \right) \quad R_{13} = \sqrt{3} \left(\frac{\sigma_{13}^y}{\sigma_y} \right) \quad (12,13)$$

For the anisotropic SX Mar-M-247, the directional yield stress ratios and coefficients were defined along the primary crystallographic orientation as:

$$F = G = H = \frac{1}{2} \quad (14)$$

$$L = M = N = \frac{3}{2} \left(\frac{R_p^{<111>}}{R_p^{<100>}} \right)^{-2} \quad (15)$$

based on modeling work performed by Ramaglia et. al. [19]. A power law hardening equation was used to account for the change in yield stress with the buildup of plastic strain [18]. The power law equation defined the current yield stress σ_y as:

$$\frac{\sigma_y}{\sigma_0} = \left(\frac{\sigma_y}{\sigma_0} + \frac{3G}{\sigma_0} \varepsilon \right)^N \quad (16)$$

where G is the shear modulus, ε is the accumulated equivalent plastic strain, σ_0^y is the initial yield stress, and N is an experimentally determined exponent. Values of σ_0^y and N were taken from modeled SX work done at the University of California Santa Barbara (UCSB) [17].

The accuracy of the plasticity model was verified through the modeling and experimental creep of a Mar-M-247 SX dog bone. The creep experiment was done at UCSB using the procedure described in Goodlet et al. [17]. The dog bone was iteratively crept to a total of 17.5% creep strain and removed at intervals to make PCRT measurements. These creep results were used to verify the accuracy of the plasticity model. The model showed excellent agreement of creep strain's effects on resonance. Figure 3 compares the change in frequency from the undeformed state to 8.9% creep strain in the modeled and measured data. While a slight offset exists between the measured and modeled frequencies, the overall pattern was consistent because the measured and modeled resonance sensitivities were the same. The measured creep data include a global frequency shift of approximately +0.3% after the first creep increment, which was not anticipated by the models. A similar global increase in resonance was reported after the first creep

increment of polycrystalline Mar-M-247 dog bone by Goodlet et al., who postulate these observations may be due to changes in material microstructure or the residual stress state of the part [17].

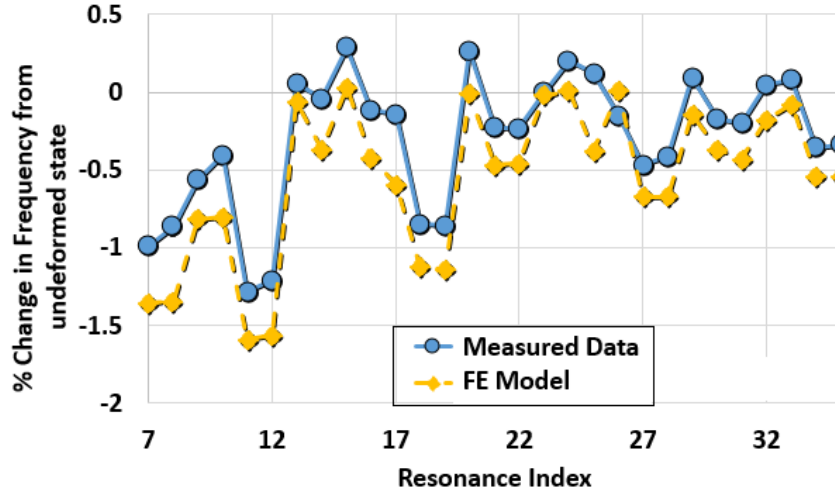


FIGURE 3. Frequency changes in crept physical and modeled dog bones

In this study, the modeled training set included 150 nominal blades (good), 44 blades with creep damage (bad), and 13 blades with crystal orientation defects (bad). Both the good and bad training sets included combined variations in geometric and material properties. Table 1 lists the input parameters and ranges used in the generation of the training set. To create the training sets, a Monte Carlo (MC) sampling randomly selected combinations of the variables, within the ranges and distributions specified, to generate each model point. A series of one-factor-at-a-time (OFAT) studies were used to set the bounds for the distributions that the MC design points were drawn from. Parameter ranges were determined through a combination of expected machining tolerances, casting variations, and previous modeling and material analysis of SX dog bone populations [6, 20, 21]. Within each range, properties were given normal distributions except for the crystal orientation parameters which were given Weibull distributions.

TABLE 1. Model input parameters and ranges used for modeled training set

	Parameter	Range for Good Parts	Range for Bad Parts
Geometric Parameter	Airfoil Thickness (Offset)	± 0.01 cm	± 0.01 cm
	Airfoil Span	± 0.0254 cm	± 0.0254 cm
	Core Thickness (Offset)	± 0.01 cm	± 0.01 cm
	Core Shift	± 0.01 cm (LE \rightarrow TE)*	± 0.01 cm (LE \rightarrow TE)*
		± 0.01 cm (P \rightarrow S)**	± 0.01 cm (P \rightarrow S)**
Material Parameter	Modulus $E_{\langle 001 \rangle}$	2%	2%
	Poisson's Ratio $\nu_{\langle 001 \rangle}$	2%	2%
	Anisotropy Ratio	2%	2%
	Density	0.20%	0.20%
Defect/Damage	ω, θ, P Crystal Orientation	$45 \pm 35^\circ, 0^\circ-15^\circ, 0-45^\circ$	$45 \pm 65^\circ, 0^\circ-17^\circ, 0-90^\circ$
	Creep Strain	0	0-5% Strain

*Leading Edge to Trailing Edge Direction **Pressure to Suction Side Direction

OFAT studies also examined how different frequencies exhibit different levels of sensitivity to various parameters. For example, Fig. 4 shows the frequency changes with model creep and model crystal orientation changes in a blade. While creep showed a decrease in frequency, different rotations (in the θ, P angles) can give different

resonance effects. Statistical analysis of these resonance pattern changes can assist in determining which parameters have changed.

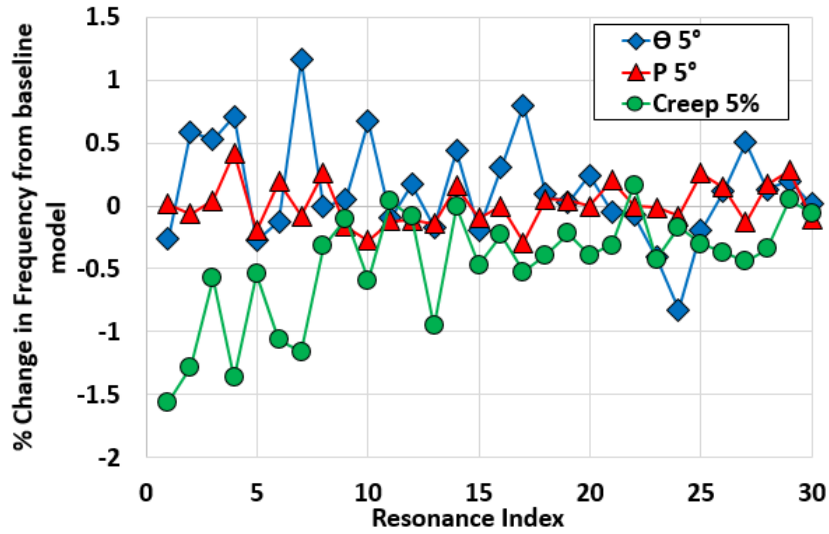


FIGURE 4. Frequency changes in blade models with crystal orientations (θ and P) and creep

RESULTS

MC Population Characteristics

The forward modeling frequency results were imported into a virtual PCRT database for analysis. Figures 5-7 show the spread of frequency variations for the first 20 resonance frequencies in the modeled good and bad parts. In these plots, the black line represents the median frequency change from the baseline/nominal model, for all the simulations. The blue band indicates the 0.25 to 0.75 percentile of the full range of variation. The dark green band shows the 0.10 to 0.90 percentile of the full range. Compared to the nominal population (Fig. 5), the creep population (Fig. 6), has shifted down in mean resonance frequency. This behavior was also observed for creep in dog bone geometries [7,17]. The blade crystal defect populations (Fig. 7), have an increased variance compared to the nominal and crept population.

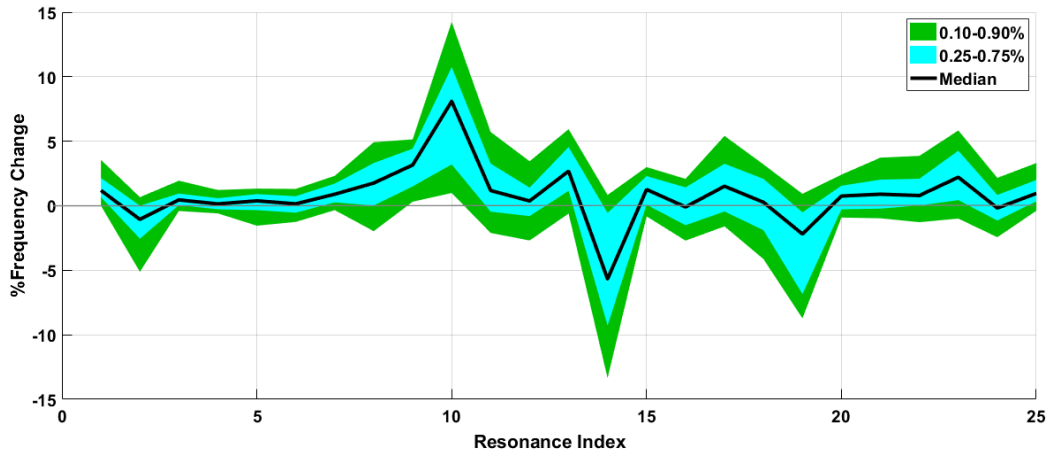


FIGURE 5. MC Frequency distribution plot for nominal blade population. The black line represents the median frequency change, the blue indicates the 0.25 to 0.75 percentile of the full range of variation, the dark green band shows the 0.10 to 0.90 percentile of the full range

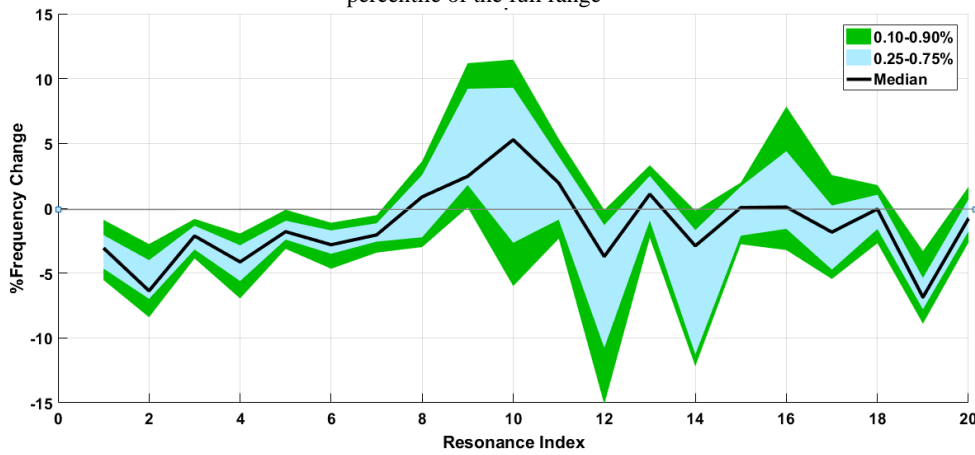


FIGURE 6. MC Frequency distribution plot for crept blade population. The black line represents the median frequency change, the blue indicates the 0.25 to 0.75 percentile of the full range of variation, the dark green band shows the 0.10 to 0.90 percentile of the full range

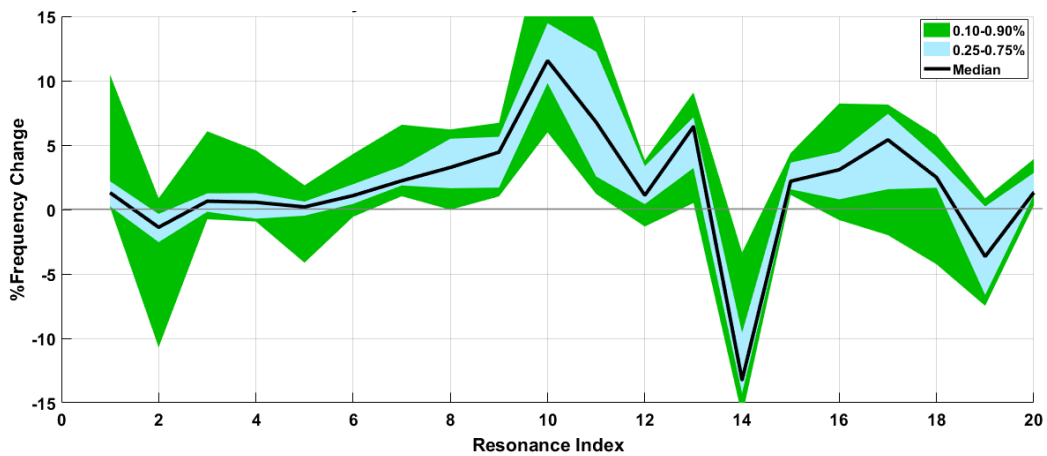


FIGURE 7. MC Frequency distribution plot for crystal defect blade population. The black line represents the median frequency change, the blue indicates the 0.25 to 0.75 percentile of the full range of variation, the dark green band shows the 0.10 to 0.90 percentile of the full range

The ranges of frequency variation predicted by the MC analysis were compared to populations of measured turbine blade PCRT data for verification. Figure 8 shows a comparison of normalized variance seen in multiple measured populations compared to the modeled good population used for the training set. In measured blade populations, a 0.5-1.5% frequency distribution was seen, depending on the blade. Overall, the modeled data spread was a good match to the measured data considering the different geometries examined. However, knowing what defines a “good match” when comparing measured to model data can be a complicated analysis. Several uncertainty quantifications and analysis studies attempt to answer this question on similar geometries [7, 12] and are currently underway for blade populations.

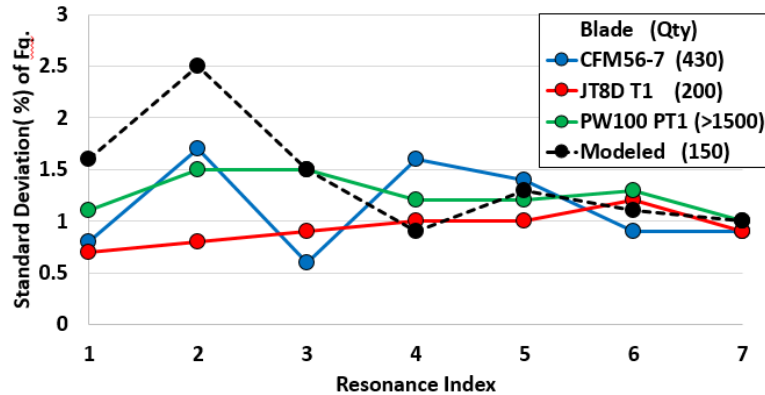


FIGURE 8. Resonance deviation (%) of frequency in measured and modeled training sets (goods)

Sorting Module Results

The forward modeling results were imported into a virtual training set database for analysis using PCRT tools. Creation of virtual spectra (via superposition of Lorentzian distributions) for each simulation also allows for a visual comparison of the model data and identification of trends. Figure 9 shows an example of seven virtual spectra created by successively increasing creep strain on each blade simulation. As creep strain increases, frequencies more sensitive to creep strain, such as frequency 15, shift more than others (e.g. frequency 16 and 17).

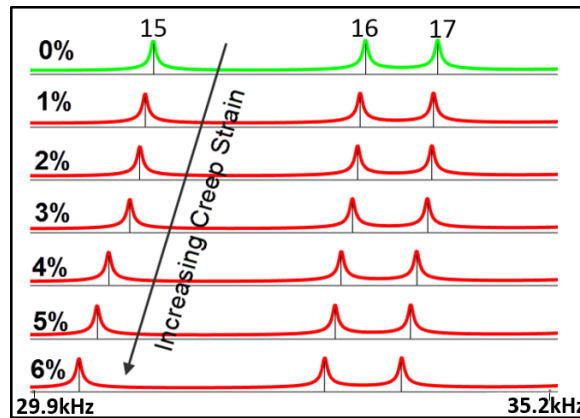


FIGURE 9. Virtual resonance spectra for frequencies 15-17 of modeled turbine blades with increasing creep strain

To create PCRT Sorting Modules that are most directly correlated to the defect severity, samples are assigned to various weighted bins, based on the degree of defectiveness. To build the targeted creep Sorting Module, the crept parts were separated into five bins based on severity of creep strain at 1-1.6%, 2.-2.6%, 3-3.7%, 4-4.9% and 5-5.7%, with a weight level on each bin of 1-5 respectively. VIPR examined the first 25 resonance frequencies and identified several diagnostic resonance frequency combinations to differentiate the good and bad parts. A creep Sorting Module was developed and each part was given an MTS and Bias score calculated from four frequencies (#2, 4, 18, 20). As

shown in Fig. 10a, all the nominal parts passed and all of the crept parts failed this inspection. Qualitatively, as creep strain increases, the MTS score increases. In addition to the PASS/FAIL nature of the inspection, this technique could lead to a quantitative evaluation of creep strain. Model validation and quantitative creep evaluations using MTS are ongoing.

Similar to the creep populations, the crystal orientation defects were assigned to severity bins, and diagnostic patterns were optimized with VIPR from the first 25 resonance frequencies. Using four frequencies (#4, 5, 10, 19) a Sorting Module correctly sorted all the nominal parts from the crystal defect parts (Fig. 10b). Qualitatively, the various crystal orientation types appeared to cluster somewhat, due to their resonance similarities. For example, defects with high θ gave high MTS scores, meaning less similarity to the goods. However, the ω and P defects were “Bias fails” and score in the bottom right quadrant. Bias fail parts look like each other, however are less different from the goods (then the high θ parts, for instance). Increasing the number of modeled crystal defect parts may make these trends more obvious.

The modeled training set was based on a generic blade model geometry, so both Sorting Modules cannot be used in field testing for known physical parts. However, if the modeling study were to be repeated based on physical blade geometries, similar virtual trained Sorting Modules are expected.

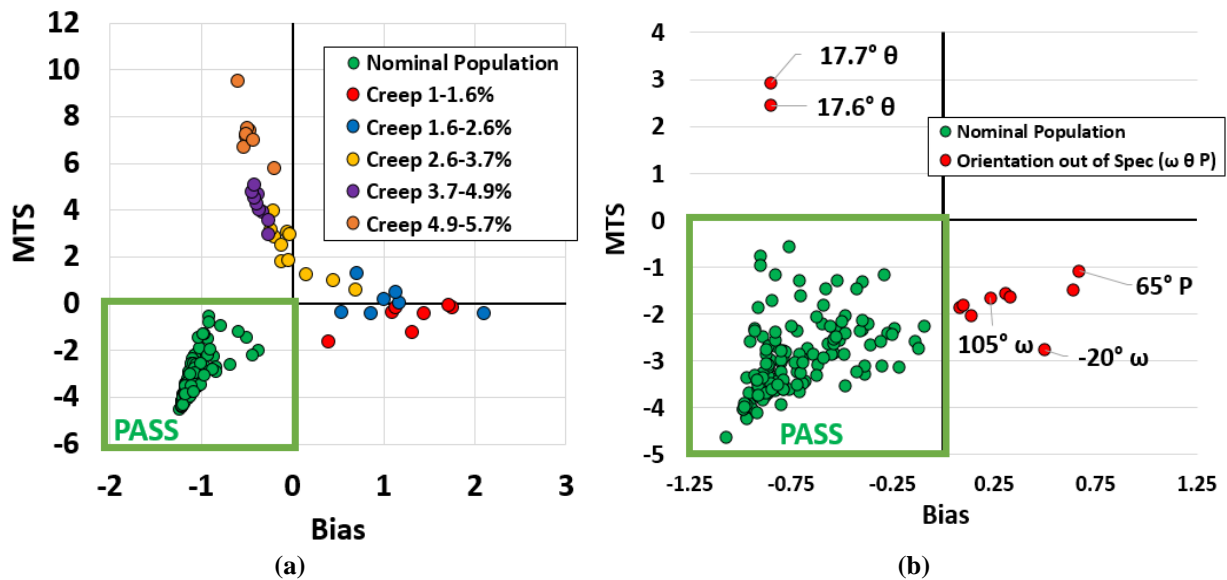


FIGURE 10. VIPR Sorting Module results for blade models (trained with virtual data) detecting (a) creep and (b) crystal defects

CONCLUSIONS AND FUTURE WORK

This work demonstrates that PCRT inspections can be created that are capable of distinguishing between creep damage and crystallographic misalignment from nominal parts in the presence of expected production variations using modeled SX turbine blades. Collecting a statically significant number of fully characterized parts for a PCRT training set is often not possible or economically feasible. To overcome this limitation, a model-assisted PCRT approach can use virtual good and bad parts to configure PASS/FAIL inspections. This work specifically examined turbine blade creep and SX crystallographic misalignment through an FEM approach. Creep modeling results were compared to experimentally crept dog bone samples with good agreement. Additionally, MC generated populations of the generic blade geometry were compared to measured data from several blade geometries currently in service, also with good agreement.

Before a virtually trained Sorting Module can be used for field-testing, a larger scale validation process is needed. Future work will include 1) large-scale validation of the model accuracy in predicting resonance frequency change due to creep damage or crystal orientation defects, 2) characterization of the inspection performance of a virtually trained inspection compared to an inspection trained with physical parts, and 3) expanding forward modeling capabilities to accurately model the resonance frequency changes due to other types of damage/defects of interest. Work is currently ongoing to address these issues.

ACKNOWLEDGMENTS

This research was supported by the U.S. Air Force Research Laboratory (AFRL) through a Materials and Manufacturing Directorate (AFRL/RX) Structural Materials Broad Agency Announcement (BAA) Contract FA8650-15-M-5208 and an AFRL Small Business Innovation Research (SBIR) Phase II Contract, FA8650-15-M-5074. This paper has been cleared for public release by AFRL under case number 88ABW-2017-5102.

REFERENCES

1. A. Migliori, J. Sarrao, M. W. Visscher, T. Bell, M. Lei, Z. Fisk, and R. Leisure, "Resonant ultrasound spectroscopy techniques for measurement of the elastic moduli of solids," *Physica B*, **183**, 1–24 (1993).
2. A. Migliori, and J. L. Sarrao, *Resonant Ultrasound Spectroscopy*, New York, Wiley, (1997).
3. J. Schwarz, J. Saxton, and L. Jauriqui, "Process compensated resonant testing in manufacturing process control," *Material Evaluation*, **63**, pp. 736-739, (2005).
4. D. Piotrowski, L. Hunter, and T. Sloan, "Process compensated resonance testing JT8D-219 1st Stage blades," ATA NDT Forum, http://www.vibrantndt.com/wp-content/uploads/75_2008_ATA_NDT_Forum-PCRT_of_JT8D-T1_Blades1.pdf (2008).
5. ASTM Standard E2534-15, "Standard practice for process compensated resonance testing via swept sine input for metallic and non-metallic parts", ASTM International, www.astm.org, (2015).
6. J. Heffernan, L. Jauriqui, E. Biedermann, A. Mayes, R. Livings, B. Goodlet, S. Mazdiyasi, "Process compensated resonance testing models for quantification of creep damage in single crystal nickel-based superalloys" *Materials Evaluation*, **75**, No. 7, pp. 941-952, (2017).
7. E. Biedermann, J. Heffernan, A. Mayes, G. Gatewood, L. Jauriqui, G. Goodlet, T. Pollock, C. Torbet, J. Aldrin, S. Mazdiyasi, "Process compensated resonance testing modeling for damage evolution and uncertainty quantification", *43rd Annual Review of Progress in QNDE*, **36**, (2017).
8. W. Woodall, R. Koudelik, K. Tsui, S. Kim, Z. Stoumbos, C. Carvounis, "A review and analysis of the Mahalanobis-Taguchi system". *Technometrics*, **45**(1), 1-15, (2003).
9. P. Mahalanobis, "On the generalized distance in statistics", *Proceedings of the National Institute of Sciences of India*, **2**, n1, pp. 49-55, (1936).
10. Solidwoks Release 2016, Dassault Systèmes, Waltham, Massachusetts, USA.
11. ANSYS Mechanical, Release 18.1.
12. E. Biedermann and L. Jauriqui "Uncertainty quantification in modeling and measuring components with resonant ultrasound spectroscopy", AFRL-RX-WP-TR-2015-0003, (2015).
13. C-M. Kuo "Effects of disoriented grains on the elastic constants of directionally solidified superalloys", *Materials Science and Engineering*, **49A**, 1-2, pp. 103-112, (2008).
14. K. Clay, J.D. Jackson, P.N. Quested, and R. Morrell "Improving single-crystal orientation determination for advanced nickel-based alloys", NPL Measurement Good Practice Guide No. 112, National Physical Laboratory, Middlesex, UK, ISSN 1368-6550, (2009).
15. C. Meher-Homji and G. Gabriele, "Gas turbine blade failures- causes, avoidance, and troubleshooting" *Proceedings of the 27th Turbomachinery Symposium*, Turbomachinery Laboratories, Texas A&M University, Houston, Texas, September 22-24, (1998).
16. W. Callister (ed) *Materials Science and Engineering: An Introduction*, Wiley, (2013).
17. B. Goodlet, C. Torbet, E. Biedermann, L. Jauriqui, J. Aldrin, and T. Pollock "Forward models for extending the mechanical damage evaluation capability of resonant ultrasound spectroscopy" *Ultrasonics*, **77**, 183-196, (2017).
18. I. Sheldon "Hill's Potential" Memo Number ST10808A, ANSYS Release 11.0, (2008).
19. A. Ramaglia and P. Villari, "Creep and fatigue of single crystal and directionally solidified nickel-base blades via a unified approach based on Hill48 potential function: Part I Plasticity and Creep," ASME Turbo Expo, (2013).
20. G. Moneta, J. Jachimowicz, and J. Osinski, "Influence of manufacturing tolerances on vibration frequencies of turbine blades" *Machine Dynamics Research*, **38**, No 1, pp. 105-118, (2014).
21. E. Hsia "Sensitivity of turbine blade temperature to tolerances of design variables" ASME presentation at the Gas Turbine Conference & Products Show, **3**, March 9-12, 1981, Houston, Texas, (1981).